Evaluation and Future Projection of Chinese Precipitation Extremes Using Large Ensemble High-Resolution Climate Simulations

WEILI DUAN,[a] NAOTA HANASAKI,[b] HIDEO SHIOGAMA,[b] YANING CHEN,[a] SHAN ZOU,[a,c] DANIEL NOVER,[d] BOTAO ZHOU,[e] AND YI WANG[a]

[a] *State Key Laboratory of Desert and Oasis Ecology, Xinjiang Institute of Ecology and Geography, Chinese Academy of Sciences, Urumqi, China*
[b] *Center for Global Environmental Research, National Institute for Environmental Studies, Tsukuba, Japan*
[c] *University of Chinese Academy of Sciences, Beijing, China*
[d] *Department of Engineering, University of California, Merced, Merced, California*
[e] *Collaborative Innovation Center on Forecast and Evaluation of Meteorological Disasters/Key Laboratory of Meteorological Disaster, Ministry of Education, Nanjing University of Information Science and Technology, Nanjing, China*

(Manuscript received 21 July 2018, in final form 21 December 2018)

ABSTRACT

Evaluation of Chinese precipitation extremes is conducted based on large ensemble projections of the present climate and 4-K-warmer climates derived from a high-resolution atmospheric general circulation model. The model reproduced the overall trend and magnitude of total precipitation and extreme precipitation events for China reasonably well, revealing that this dataset can represent localized precipitation extremes. Precipitation extremes are more frequent and more severe in future projections under 4-K-warmer climates than in the representative concentration pathway 8.5 (RCP8.5) scenario of phase 5 of the Coupled Model Intercomparison Project (CMIP5). Our results show that using a large-ensemble simulation can improve the ability to estimate with high precision both the precipitation mean and the precipitation extremes compared with small numbers of simulations, and the averaged maximum yearly precipitation will be likely to increase by approximately 18% under a +4-K future in southern China compared with the past. Finally, uncertainty evaluation in future precipitation projections indicates that the component caused by the difference in six ΔSST patterns is more important in southern China compared with the component due to the atmospheric internal variability. All these results could provide valuable insights in simulating and predicting precipitation extremes in China.

1. Introduction

As the global climate changes, natural disasters caused by extreme weather events are becoming more frequent and leading to increasingly serious consequence around the world (Seneviratne et al. 2012; Christidis et al. 2015; Fischer and Knutti 2015). China is vulnerable to extreme weather events (Sun et al. 2014; Duan et al. 2016; Wu et al. 2019). Thus, some researchers have investigated and evaluated the changes of climate extremes in China (Zhang et al. 2006; Ji and Kang 2015; Tang et al. 2016). Based on the global climate model (GCM) outputs derived from phases 3 and 5 of the Coupled Model Intercomparison Project (CMIP3 and CMIP5, respectively), most of these studies generally indicate that cold weather extremes exhibit a decreasing trend, warm weather extremes show an increasing trend, and extreme heavy precipitation is likely to become more severe (Chen et al. 2012; Zhou et al. 2014; Li et al. 2017). However, most of these results only reflect one or several GCM models with relatively coarse resolution (>100 km). To date, detailed analysis of large ensemble climate simulations with high-resolution GCMs for China has been limited.

The variabilities of the extreme events are generally larger than the mean climate state (e.g., the annual maximum daily precipitation has larger variance than the annual mean precipitation). Large variances of extreme events would produce hurdles in making robust

Supplemental information related to this paper is available at the Journals Online website: https://doi.org/10.1175/JCLI-D-18-0465.s1.

Corresponding author: Yaning Chen, chenyn@ms.xjb.ac.cn

DOI: 10.1175/JCLI-D-18-0465.1

projections of the future changes using small size ensembles of the climate model simulations (Li et al. 2015; Mote et al. 2016). To overcome this hurdle, Mizuta et al. (2017) have recently produced a large ensemble climate simulation with a high-resolution atmospheric model—the ''Database for Policy Decision-Making for Future Climate Change'' (d4PDF). This effort is similar to weather@home with large regional ensemble simulations (Massey et al. 2015; Schaller et al. 2016; Freychet et al. 2018). The d4PDF database represents over 5000 years of ensemble future climate simulation (90 ensembles × 60 years) using a 60-km-resolution atmospheric general circulation model (MRI-AGCM3.2) and dynamical downscaling around Japan with a 20-km-resolution nonhydrostatic regional climate model (NHRCM), providing larger ensembles and higher horizontal resolution than earlier projections (usually coarser than 100 km) (Collins et al. 2013), in which six climatological sea surface temperature (SST) warming patterns (ΔSSTs) from CMIP5 climate models are added to the observed SST data to make the lower boundary conditions to cover the most part of the uncertainty of the patterns in all the CMIP5 models. These features enable us to further explore variations of regional and global extreme weather events as well as their uncertainty (Mizuta et al. 2017).

Studies based on the d4PDF database are rapidly appearing (Matsueda and Endo 2017; Mizuta et al. 2017; Yoshida et al. 2017). For example, Shiogama et al. (2016) investigated the impacts of human activities on historical changes in extreme weather events. Imada et al. (2017) examined future changes in precipitation extremes in East Asia and discussed their uncertainty through an analysis of differences of internal variability (including decadal variations in the ocean and intraseasonal variation in the tropics) and differences among future SST patterns. All in all, these studies suggest a good performance in simulating climatology as well as extremes by using these high-resolution AGCMs. However, most of them focus regionally based on very few indices of extreme events. Further research should be done to explore the benefits of the large high-resolution ensemble.

The objectives of this study are 1) to evaluate the quality of the d4PDF large ensemble in simulating precipitation extremes by comparing with an observed high-resolution-grid dataset in China, 2) to investigate future changes in precipitation extremes under 4-K global warming, and 3) to discuss future projection uncertainty from internal variability and future SST patterns. The paper begins with a brief description of the datasets and methodology in section 2, followed by the results of precipitation extreme indices and a discussion, presented in section 3, followed by conclusions in section 4.

2. Experimental design, data, and methods

a. Experimental design of d4PDF

The d4PDF consists of two parts: one is the global climate simulations derived from a 60-km-resolution AGCM (MRI-AGCM3.2; Mizuta et al. 2012) and the other is the regional downscaling simulations covering Japan (20-km horizontal grid spacing; Mizuta et al. 2017). We analyzed the outputs of the global model.

Three sets of time-slice experiments including a historical climate simulation, a +4-K future climate projection, and a nonwarming simulation are performed by using the MRI-AGCM3.2. Historical climate and nonwarming simulations are comprised of 100-member ''all forcing'' (ALL) runs and 100-member ''nonwarming trends'' (NW) runs for the period from 1951 to 2010 based on initial-value perturbations of the atmosphere and short-term monthly SST perturbations. Future climate is simulated according to a constant warming condition roughly corresponding to the level of year 2090 under the representative concentration pathway 8.5 (RCP8.5) scenario adopted in CMIP5. A 60-yr integration (2051–2110) with 90 members is presented to represent the future climate in which global-mean surface air temperatures (SATs) are 4 K warmer than the preindustrial level. SST data for the future period were developed by adding CMIP5 AOGCM-projected SST anomalies (ΔSSTs) as a function of longitude, latitude, and month to observed SST after removing the long-term trend of the observed SSTs (1951–2010). Because of the large variety in future SST projections, six different ΔSSTs [CCSM4 (CC), GFDL CM3 (GF), HadGEM2-AO (HA), MIROC5 (MI), MPI-ESM-MR (MP), and MRICGCM3 (MR)] were selected using cluster analysis with tropical ΔSST spatial patterns [see Table S1 in the online supplemental material; also, please see detailed information from Mizuta et al. (2017)] to represent the range of uncertainty in CMIP5 projections. A scaling factor was multiplied for each pattern in order to produce a global-mean surface air warming of 4 K. Meanwhile, for each of the six ΔSSTs, 15-member ensembles were run using different initial atmospheric conditions and different small random perturbations on SST (δSST) (i.e., 90 members in total). Data from the historical climate simulations and +4-K future climate simulations in China are extracted for analysis in this study.

b. Other datasets

1) Observed dataset

Observed daily precipitation data from 1961 to 2010 with 0.5° × 0.5° resolution were selected to assess model performance at the regional scale for China. This dataset

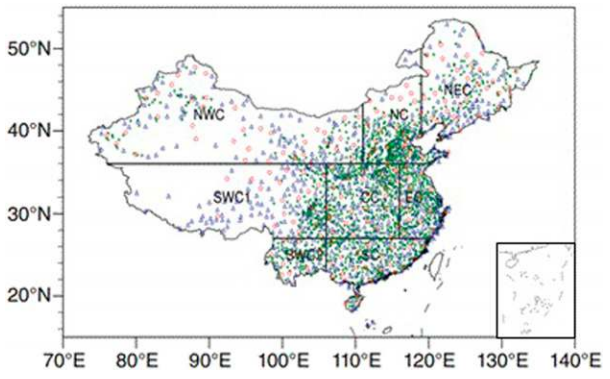

FIG. 1. Distribution of 2461 stations in China (CN) marked by red dots, blue triangles, and green asterisks that are employed for the CN05 grid dataset. The red dots indicate 196 stations used in Zhai and Pan (2003), the blue triangles indicate the added stations in the 751 stations (Xu et al. 2009) and the green asterisks indicate the newly added observing stations in the 2416 stations. The domains of eight subregions—northeast China (NEC); northern China (NC); eastern China (EC); central China (CC); southern China (SC); southwest China, region 1, or Qinghai–Tibet (SWC1); southwest China, region 2 (SWC2); northwest China (NWC)—used in the analysis are also shown. [Modified from Zhou et al. (2016).]

(hereafter referred to as CN05; see Fig. 1) was developed from 2416 weather monitoring stations charged by the National Climate Center, China Meteorological Administration (Wu and Gao 2013), which has a larger number of stations compared to the previous 196 stations (Zhai and Pan 2003) and 751 stations (Xu et al. 2009). But the distribution of stations exhibits a diminishing scale from east to west and from south to north; especially, it has sparse distribution in northwest China (NWC) and Qinghai–Tibet (SWC1). Using the method of ''anomaly approach'' (New et al. 2000), the CN05 grid dataset was constructed based on the gridded daily anomaly and the gridded climatology [detailed steps can be found in Wu and Gao (2013)]. Because of higher accuracy and resolution, the CN05 has been employed successfully in describing more detailed information of regional climate change and validating high-resolution climate model (Wu and Gao 2013).

2) CMIP5 DATASETS

To better analyze performance of d4PDF simulations, precipitation extremes from CMIP5 were used to compare with d4PDF. CMIP5 provides a framework for coordinated climate change experiments based on dozens of GCMs under four representative concentration pathway (RCP) scenarios, but has a coarse spatial resolution and a low number of ensembles for each model, which is difficult to disentangle uncertainty from model formulation differences and internal climate variability (Kay et al. 2015). A single (the first) ensemble member of 34 models from CMIP5 (see Table S2 for full list of expansions) was used in this study. All the precipitation extreme indices from CMIP5 simulations can be downloaded online (http://www.cccma.ec.gc.ca/data/climdex/index.shtml; accessed March 2018).

c. *Methodology*

1) COMPUTATION OF CLIMATE INDICES AND DATA PROCESSING

To describe and assess climate extremes, 27 widely used climate indices were developed and recommended by the Expert Team on Climate Change Detection and Indices (ETCCDI) (available at https://www.climdex.org/learn/indices/) (Zhang et al. 2011; Sillmann et al. 2013; Duan et al. 2015). In this study, six indices (Table 1) including the annual total wet-day precipitation (PRCPTOT), the maximum number of consecutive dry days (CDD), the annual maximum 1-day precipitation (RX1day), the annual total precipitation divided by the number of wet days (SDII), the annual number of heavy precipitation days (R10mm), and the annual total precipitation on extremely wet days (R99p) were selected and computed on an annual basis for observation data (CN05), historical climate simulations (d4PDF and CMIP5), and +4-K future climate simulations (d4PDF) to analyze extremes and detect future precipitation variations in China.

Because of different resolutions between different datasets, we regridded all precipitation indices to a common 116 × 71 grid (about 0.5625° × 0.5625°) for China using a remapping procedure (Jones 1999). According to administrative boundaries and societal and geographical conditions, we examined changes of spatial patterns from eight regions including northeast China (NEC), northern China (NC), eastern China (EC), central China (CC), southern China (SC), southwest China (SWC2), northwest China (NWC), and Qinghai–Tibet (SWC1) (Fig. 1 and Table 2) (National Report Committee 2007).

2) PERFORMANCE METRICS

To examine the performance of the AGCM precipitation simulations in China, we first compared the seasonal mean precipitation simulations with the gridded observed precipitation averaged for the period 1981–2005. The season was divided into winter [December–February (DJF)], spring [March–May (MAM)], summer [June–August (JJA)], and autumn [September–November (SON)]. Taylor diagrams (Taylor 2001) were applied to assess model performance for the precipitation indices to present a concise statistical summary, suggesting matching

TABLE 1. Definitions of six precipitation indices used in this study. RR is daily precipitation. A wet day is defined when RR ≥ 1 mm, and a dry day when RR < 1 mm.

ID	Indicator name	Definition	Unit
PRCPTOT	Annual total wet-day precipitation	Annual total PRCP in wet days (RR ≥ 1mm)	mm
CDD	Consecutive dry days	Maximum number of consecutive days with RR < 1mm	day
RX1day	Max 1-day precipitation amount	Annual maximum 1-day precipitation	mm
SDII	Simple daily intensity index	Annual total precipitation divided by the number of wet days (defined as PRCP ≥ 1.0 mm) in the year	mm day^{-1}
R10mm	Number of heavy precipitation days	Annual count of days when PRCP ≥ 10mm	day
R99p	Extremely wet days	Annual total PRCP when RR > 99th percentile of precipitation on wet days in the 1961–90 period	mm

degrees between the observed and simulated spatial patterns through calculating correlation, root-mean-square difference (RMSD) and ratio of their variances with respect to observations.

3) CLIMATE CHANGE PROJECTIONS

The 20-yr time-slice future projections (2081–2100) were compared to historic simulations to clarify future changes in precipitation indices. The baseline historic simulation reflects the period from 1981 to 2000. Precipitation changes are computed as the relative change C_R (%) between the projection period and baseline period, according to the following equation:

$$C_R = \frac{\text{Projection} - \text{Baseline}}{\text{Baseline}}. \tag{1}$$

The ensemble change is computed as the mean of 100 (90) ensembles for the historical (future) runs for 60 years, and box-and-whisker plots are used to show projected changes in the annual precipitation indices. In addition, to reveal advantages of large ensembles for evaluating extreme precipitation events, the single ensemble and multiple ensembles are compared for all of China.

4) ANALYSIS OF VARIANCE

Here, we applied a two-way analysis of variance (ANOVA) (Sugi et al. 1997; Endo et al. 2017) to decompose the total variance $\hat{\sigma}^2_{\text{tot}}$ of future precipitation extremes into that of the difference in six ΔSST patterns $\hat{\sigma}^2_{\Delta\text{SST}}$ and the internal variability of the 15 δSST ensemble $\hat{\sigma}^2_{\text{int}}$:

$$\hat{\sigma}^2_{\text{tot}} = \hat{\sigma}^2_{\Delta\text{SST}} + \hat{\sigma}^2_{\text{int}}, \tag{2}$$

where $\hat{\sigma}^2_{\text{int}}$ represents the variance of the deviation of given data from the ensemble mean of different atmospheric initial conditions and δSST values, and $\hat{\sigma}^2_{\Delta\text{SST}}$ indicates the variance associated with the difference in six ΔSST patterns, in which the variance of the ensemble mean of different atmospheric initial conditions and δSST values $\hat{\sigma}^2_{\text{EM\_}\delta\text{SST}}$ is corrected by extracting the effect of internal variability. They can be estimated by Eqs. (3)–(5):

$$\hat{\sigma}^2_{\text{int}} = \frac{1}{N(n-1)} \sum_{i=1}^{N} \sum_{j=1}^{n} (x_{ij} - \overline{x}_i)^2, \tag{3}$$

$$\hat{\sigma}^2_{\text{EM\_}\delta\text{SST}} = \frac{1}{N-1} \sum_{i=1}^{N} (\overline{x}_i - \overline{\overline{x}})^2, \tag{4}$$

$$\hat{\sigma}^2_{\Delta\text{SST}} = \hat{\sigma}^2_{\text{EM\_}\delta\text{SST}} - \frac{1}{n}\hat{\sigma}^2_{\text{int}}, \tag{5}$$

where N represents the number of different ΔSSTs (i.e., $N = 6$) and n is the number of ensemble members with different atmospheric initial conditions and δSSTs (i.e., $n = 15$). Here, x_{ij} represents the future change rate (%) of a climatological-mean precipitation index for the ith ΔSST pattern and jth member of the ensemble of different initial conditions and δSST values. Variable $\overline{x}_i$ is the ensemble mean of the ith ΔSST, and $\overline{\overline{x}}$ is the average

TABLE 2. Coordinates of the eight subregions and the whole of China used in this study.

Name	Abbreviation	Coordinates
Northeast China	NEC	39°–54°N, 119°–134°E
Northern China	NC	36°–46°N, 111°–119°E
Eastern China	EC	27°–36°N, 116°–122°E
Central China	CC	27°–36°N, 106°–116°E
Southern China	SC	20°–27°N, 106°–120°E
Qinghai–Tibet 1	SWC1	27°–36°N, 77°–106°E
Southwest China	SWC2	22°–27°N, 98°–106°E
Northwest China	NWC	36°–46°N, 75°–111°E
Whole of China	ALL	15°–55°N, 70°–140°E

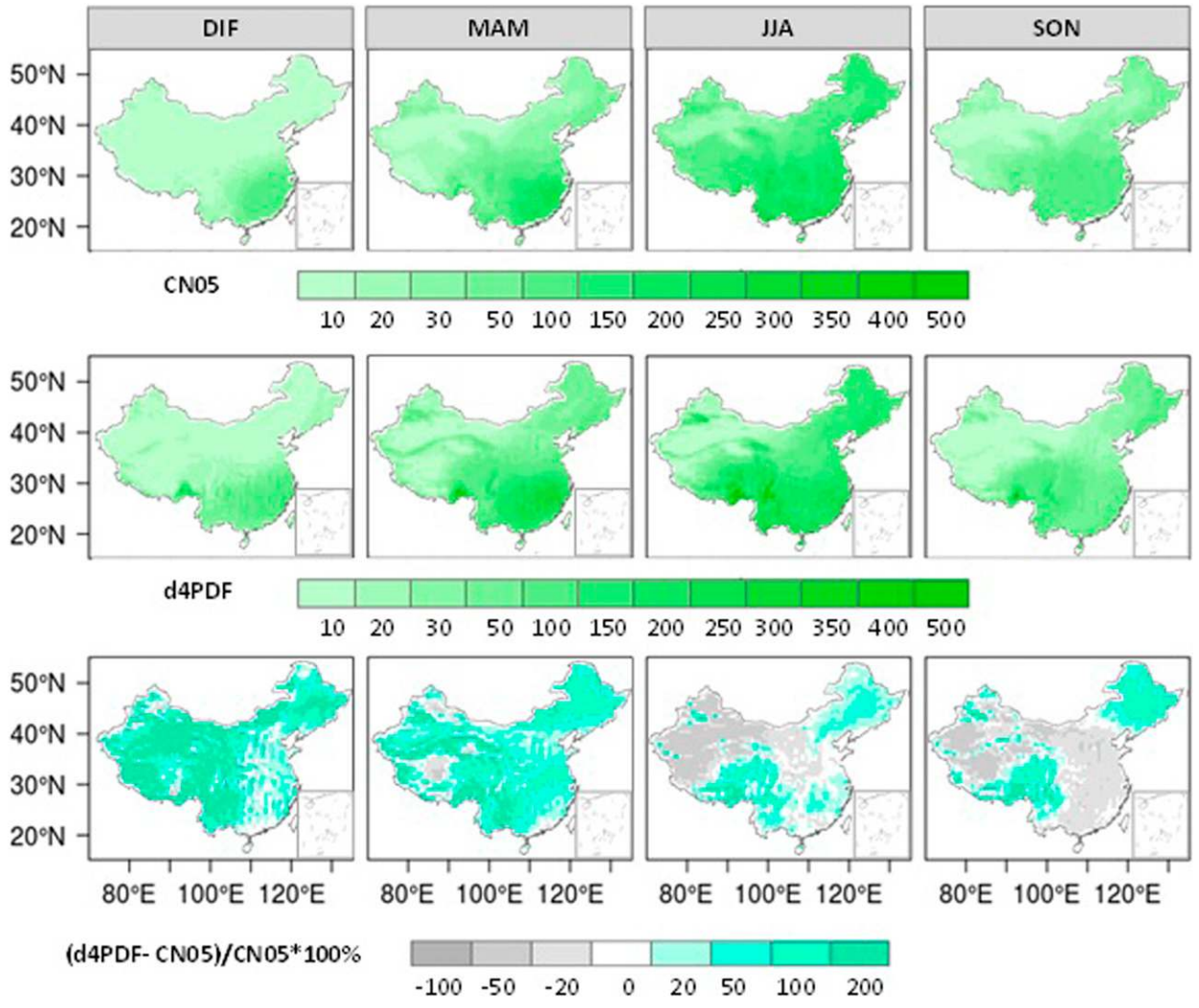

FIG. 2. Seasonal mean precipitation (mm month^{-1}) in 1981–2005 for (left to right) DJF, MAM, JJA, and SON from (top) CN05, (middle) d4PDF, and (bottom) the bias [(d4PDF − CN05)/CN05] (%).

of all data. The caret (ˆ) denotes the best estimator of a population quantity.

3. Results and discussion

a. Evaluation of the present-day simulation

1) MEAN PRECIPITATION AMOUNTS

Figure 2 compares the simulated (ensemble mean) and observed distributions of mean seasonal precipitation from 1981 to 2005, showing a reasonable reproducibility in the magnitudes of precipitation and its spatial patterns in all seasons. Precipitation over China has distinct seasonal and regional characteristics, and mainly concentrates in the southeast during spring and summer for both d4PDF and CN05 datasets because of the monsoon circulation, the amount of which are roughly greater than 500 mm yr^{-1}. The bias in percent [(d4PDF − CN05)/CN05 × 100%] was about +30% for most regions for all seasons, especially in summer (JJA) and autumn (SON). During winter, however, a distinct positive bias was found around the Tibetan Plateau, where the topography strongly affects precipitation (the average elevation generally exceeds 4000 m, with mountain ranges over 6000 m; Yin et al. 2008).

Table 3 shows the seasonal model biases for mean precipitation and mean correlation coefficients between d4PDF and CN05 time-averaged spatial fields. The bias was the largest in spring, up to 24.58 mm month^{-1}, while the smallest in autumn with the value of 0.65 mm month^{-1}. The spatial correlations for precipitation between d4PDF and CN05 were above 0.7

TABLE 3. The 25-yr average (1981–2005) seasonal precipitation (mm month^{-1}) from CN05 and d4PDF, the bias (model minus observed), and the spatial correlation R over all of China.

Season	Model	Observed	Bias	R
DJF	21.27	12.81	8.46	0.79
MAM	70.01	45.43	24.58	0.93
JJA	113.52	105.47	8.05	0.85
SON	37.84	37.19	0.65	0.70

for all seasons for China, with spring season being as high as 0.93. Figure S1 indicates that the uncentered correlations (Kiktev et al. 2007) were good for all seasons in places like eastern and central China, but had relatively low skill in southwest and northern China. These results suggest that the simulations of d4PDF reasonably captured the seasonal patterns of the observed precipitation in China.

To deeply investigate the influence of topography on simulated and observed precipitation, the winter (DJF) and summer (JJA) precipitation cross sections along 30.8°N (across the Qinghai–Tibet area) were examined. From Fig. 3, we can see that elevation (black line) shows as a decreasing "ladder," revealing that the topography of China is a three-step staircase stepping down from the Qinghai–Tibet Plateau (with the 4000-m-high mountains) in the southwest to the coastal belt in the east (below 1000 m); the precipitation gradients from d4PDF along the transect were roughly consistent with the CN05 in winter and summer, but the simulations of d4PDF were greater than the CN05 in the Qinghai–Tibet Plateau, especially in the steepest region between the first and the second staircases (around 83.8°E), suggesting relatively poor correspondences between the d4PDF simulation and the CN05 over the eastern Qinghai–Tibet Plateau. However, the observed precipitation in the Qinghai–Tibet Plateau was not perfect because of sparse meteorological stations within this region (Fig. 1). The results could be also illustrated by Fig. 2 and are consistent with the analysis of CMIP5 (Su et al. 2013), which also reflect the general weakness of rainfall prediction in GCM simulations because topography is the main influencing factor forcing rainfall patterns (Bader et al. 2008).

2) PRECIPITATION EXTREMES

To assess the extreme precipitation in d4PDF simulation, spatial distributions of mean six extreme-precipitation indices from 1981 to 2005 are presented in Fig. 4. Compared to CN05 and CMIP5, the d4PDF simulation did well in catching the climatological mean pattern of extreme precipitation events such as represented by the annual total wet-day precipitation (PRCPTOT; see Fig. 4a), the maximum number of consecutive dry days (CDD; see Fig. 4b), the annual maximum 1-day precipitation (RX1day; see Fig. 4c), the annual total precipitation divided by the number of wet days (SDII; see Fig. 4d), the annual number of heavy precipitation days (R10mm; see Fig. 4e), and the annual total precipitation on extremely wet days (R99p; see Fig. 4f). The extreme precipitation indices including PRCPTOT, RX1day, SDII, R10mm, and R99p in southeast China were greater than that in northwest China. The d4PDF simulations were generally better than CMIP5 simulations in most of China. However, d4PDF simulations in RCPTOT, RX1day, SDII, R10mm, and R99p overestimated the observations in many places, especially in the eastern Qinghai–Tibet Plateau, which are consistent with the positive bias seen in the mean precipitation amounts (see Fig. 2). In contrast, Fig. 4b shows that all simulations including d4PDF and CMIP5 underestimated CDD in most regions, especially in northwest China, although d4PDF

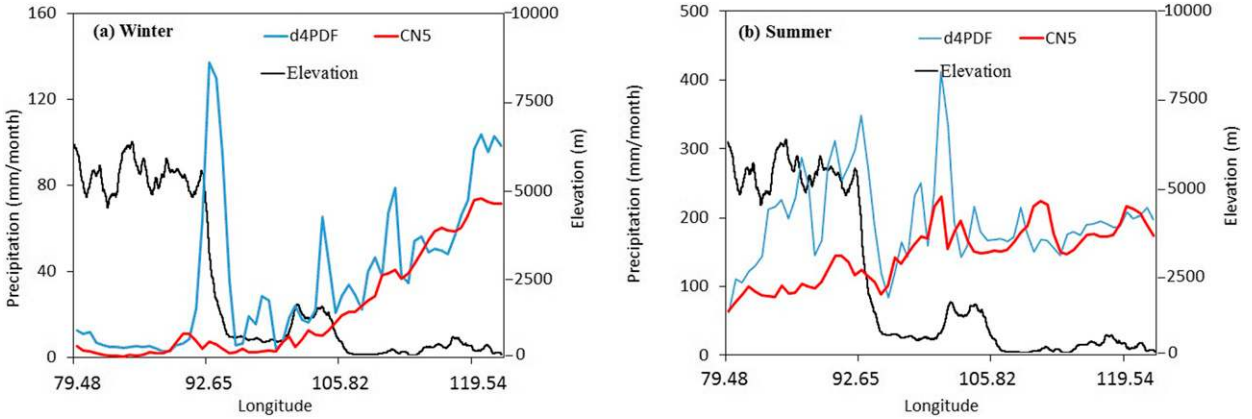

FIG. 3. Simulated d4PDF and observed CN05 (a) DJF precipitation (mm month^{-1}) and (b) JJA precipitation (mm month^{-1}) along a west–east transect at 30.8°N.

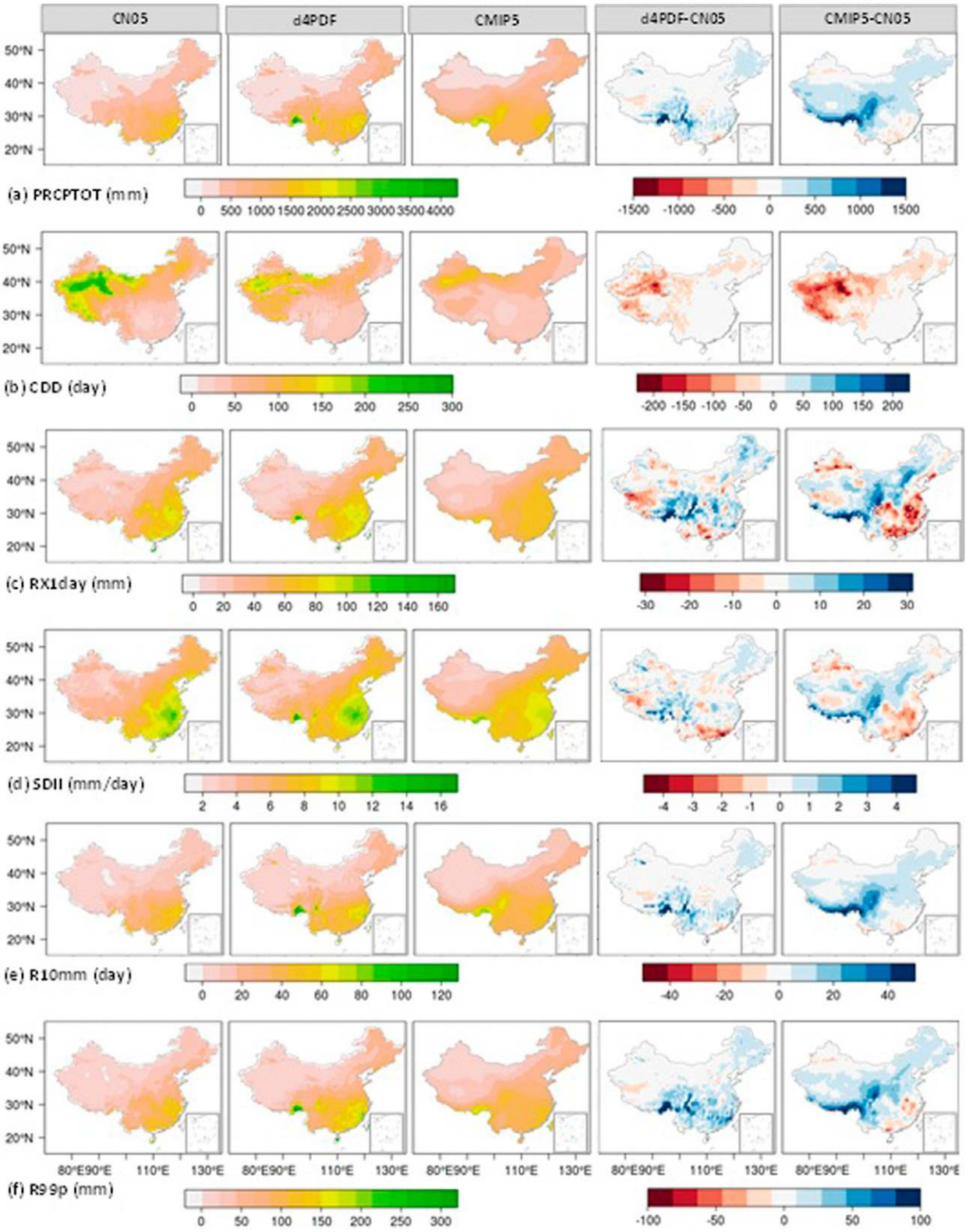

FIG. 4. The 25-yr (1981–2005) averaged (a) PRCPTOT (mm), (b) CDD (day), RX1day (mm), (c) SDII (mm day^{-1}), (d) R10mm (day), and (e) R99p (mm). (left to right) The results for CN05, d4PDF, CMIP5, d4PDF-CN05, and CMIP5-CN05 are displayed. The results for d4PDF and CMIP5 are the ensemble mean.

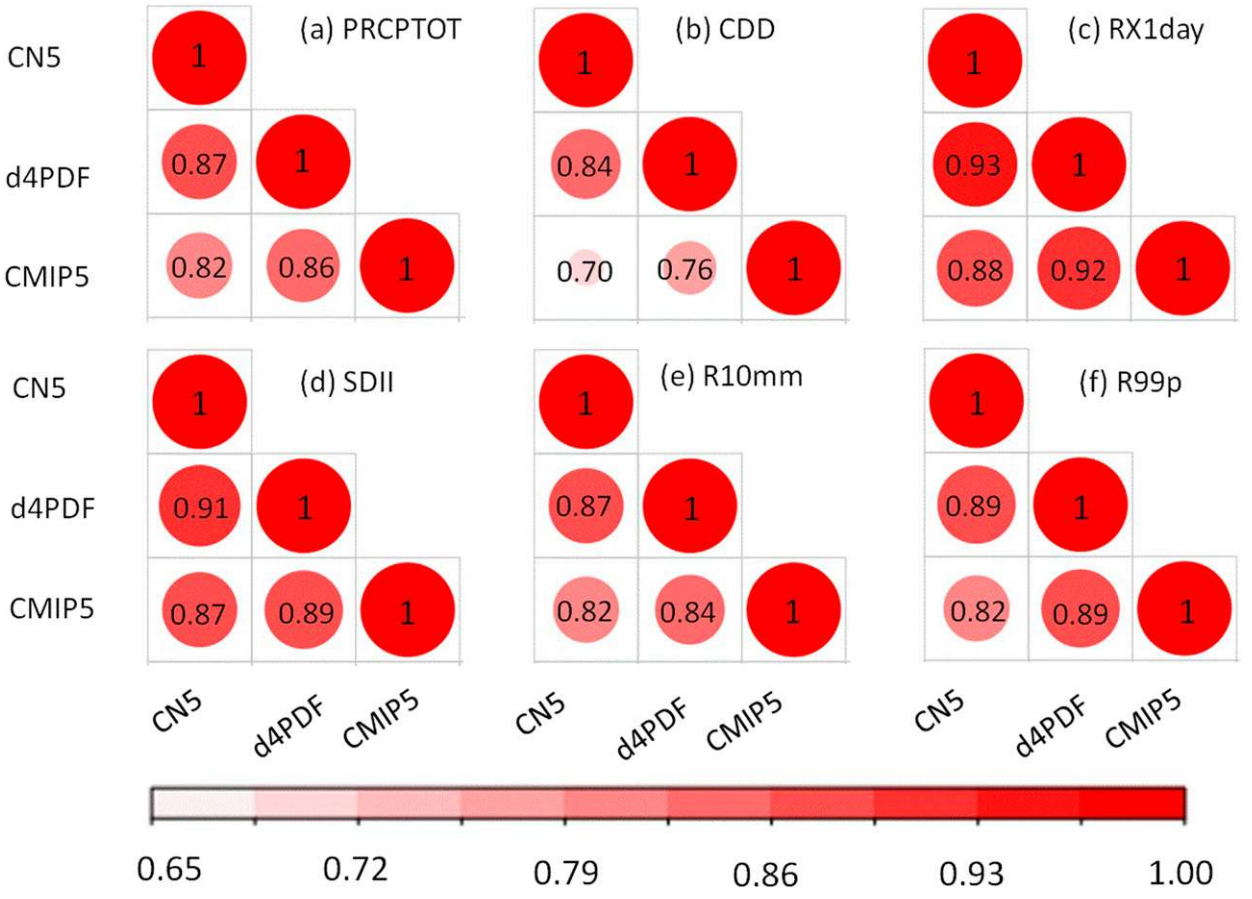

FIG. 5. Spatial correlations *R* between all pairs of datasets (CN05, d4PDF, and CMIP5) in annual-mean (a) PRCPTOT, (b) CDD, (c) RX1day, (d) SDII, (e) R10mm, and (f) R99p from 1981 to 2005. The color and size of the circles represent the magnitude of the correlation.

performs better than CMIP5. One possible reason for this is that the increase of total precipitation would be likely to contribute to the decline of CDD. Another possible cause is the common problems of climate models in producing too much light rain (e.g., drizzle).

To better evaluate the spatial distributions of mean precipitation extremes from d4PDF simulations, the spatial correlations between all pairs of datasets in mean precipitation extreme indices were calculated (Fig. 5). Figure 5 shows that the correlation matrices confirm the generally good agreement between the d4PDF simulations and CN05 dataset, with correlation coefficients *R* being above 0.85 for most extreme precipitation indices, which suggests d4PDF simulations were reliable in reflecting the spatial distribution in annual mean extreme precipitation events. Among these, RX1day (Fig. 5c) has the highest correlation coefficients with the value of 0.93, followed by SDII (0.91) and R99p (0.89) (see Figs. 5c,d,f). In addition, Fig. 5 also clearly indicates that the spatial correlations between d4PDF simulations and CN05 observations were better than those of CMIP5 simulations for all six extreme precipitation indices. For example, the spatial correlation between d4PDF simulations and CN05 observations was 0.85, while it was 0.70 between CMIP5 simulations and CN05 observations (Fig. 5b). To better represent the performance in different places between d4PDF simulations and the observed CN05 dataset, we developed Taylor diagrams for all indices in eight regions, which are shown in Fig. S2. Figure S2 indicates that the model performed relatively poorly in Qinghai–Tibet (SWC1) and southwest China (SWC2) compared to other regions, where precipitation is strongly influenced by complex topography and meteorological monitoring stations are scarce and unevenly distributed (Fig. 1).

In summary, d4PDF performs well in reproducing the spatial patterns for all six precipitation indices in China, and large ensemble simulations have tremendous advantages in investigating statistical properties for climate especially for impact-relevant extreme weather

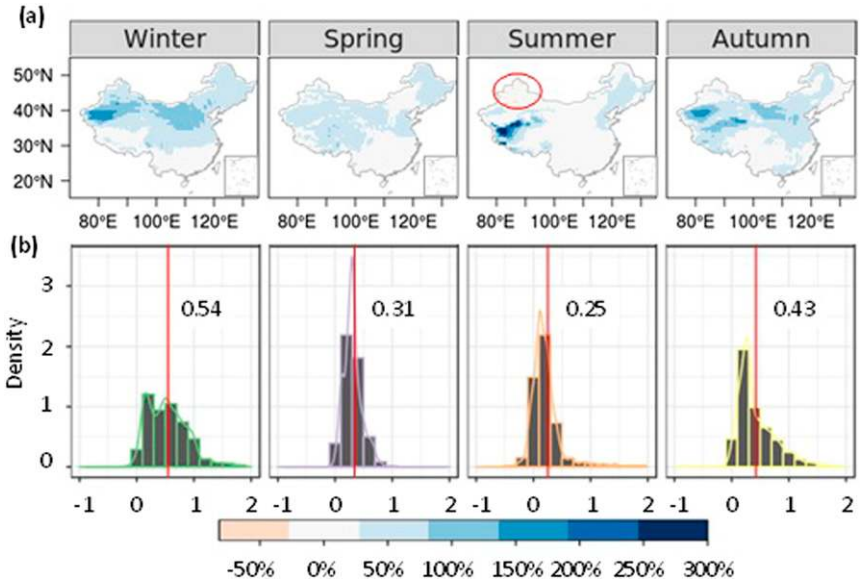

FIG. 6. (a) Spatial distribution and (b) histogram and density map of future changes (ratio) in seasonal mean precipitation over the period 2081–2100 relative to the reference period 1981–2000. The area in the red ellipse in (a) indicates where changes are negative, and the vertical red line in (b) is for mean changes.

events, compared with observed datasets alone or a handful of CMIP5 simulations.

b. Future changes

1) MEAN PRECIPITATION

Figure 6 shows the spatial distributions, histogram, and density of future changes (%) in seasonal mean precipitation over the period 2081–2100 relative to the reference period 1981–2000. Except for summer, the d4PDF future projections generally exhibited an increase of 50% over China, and the increasing amplitude was higher in the north than in the south. For example, Fig. 6a shows that the increase in most regions of the north of China was more than 50% in most seasons; in particular, a nearly double increase appeared around the Tarim River basin in winter and autumn, and a more than threefold increase occurred in the western Qinghai–Tibet Plateau in summer. Figure 6b indicates that winter had the largest mean increasing amplitude over China, up to 54%, followed by autumn (43%) and spring (31%), with the lowest mean increase in summer (25%). Compared to other seasons, winter has the lowest average seasonal precipitation. Therefore, the relative changes of precipitation in winter are likely to become very big even with a small amount of precipitation increase.

To further understand influences of SST patterns in future projections, we compared the change of mean seasonal mean precipitation between future projections (2081–2100) from each SST pattern and the historic simulations (1981–2000) (see Fig. S3). The MI SST pattern was the weakest in projections of winter precipitation compared with other SST patterns (Fig. S3a), mainly reflected in northwest China, while the MI and MP SST patterns were the strongest in projections of autumn precipitation in northwest China (Fig. S3d). Also, from Fig. S3c we can see that the sensible increase occurred in the western Qinghai–Tibet Plateau in summer may mainly come from the contribution of projections under MI and GF SST patterns.

2) PRECIPITATION EXTREMES

Changes in the spatial distribution of extreme precipitation indices for all ensemble members (100 for the historical runs and 90 for the future ones) are shown in Fig. 7. Except for CDD (Fig. 7b), the other five indices are projected to increase in the most of the country. The projected percent increases in PRCPTOT, R10mm, and R99p are larger in northwestern China than in southeastern China. Also, PRCPTOT, R10mm, and R99p will be likely to increase by 30%–50% in most regions, and even about 200% in Tibet Plateau (Figs. 7a,e,f); the consecutive dry days will be likely to increase in southern China but decrease in northern China (Fig. 7b). These tendencies are generally consistent with the results from the CMIP5 simulation (Zhou et al. 2014), but results obtained here have

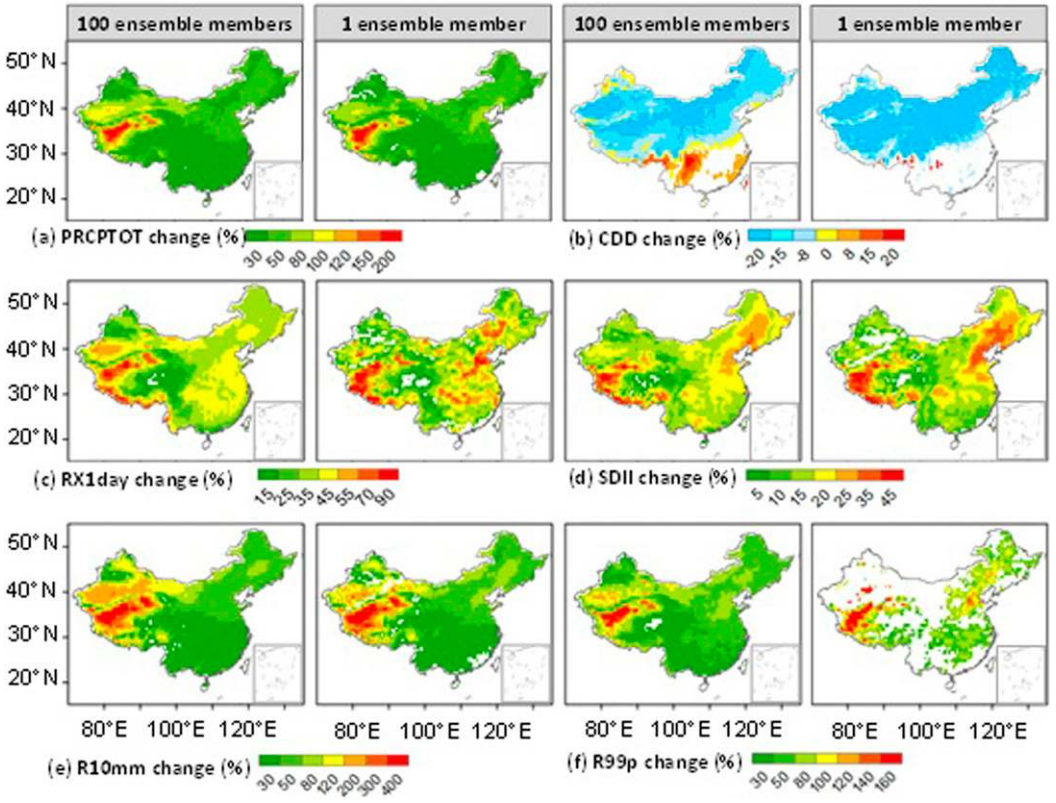

FIG. 7. Relative change (%) in precipitation indices for the future (2081–2110) for (left) 100 historical or 90 future ensemble members and (right) 1 ensemble member. The 1981–2000 period is used as the base period. Areas with white indicate where differences are not statistically significant at the 5% level using a Student's *t* test.

higher resolution, making it easier to distinguish changes for the eight subregions.

Figure 8 compares precipitation extreme indices for all of China between a historical period (1981–2000) and a future period (2081–2100). Except for CDD, the other extreme indices are projected to increase for all six SST patterns during 2081–2100, suggesting that both total precipitation amount and extreme precipitation events will be likely to increase in the future. CDD represents maximum number of consecutive days with precipitation <1 mm, so it should decrease when the number of days with precipitation >1 mm increases (Fig. 7b). The median changes of PRCPTOT is simulated to increase from 650 to 820 mm, up to approximately 26% (Fig. 8a), which is higher than the increase of averaged wet day daily amount (SDII), revealing that the main reason for increasing total precipitation is the increasing intensity of precipitation across China, not the variations of the number of wet days. The predicted percentage increases in RX1day, R10mm, and R99p are about 35% (from 44 to 54 mm), 33% (from 18 to 24 days), and 40% (from 50 to 70 mm) higher than that of PRCPTOT, suggesting a sharp increase in extreme weather events in the future and a positive contribution to the total precipitation variation due to the increased precipitation on very wet days. All changes are much higher than the results under RCP8.5 for the 24 climate models from the CMIP5 simulation (Zhou et al. 2014).

Figure 8 also clearly illustrates that future extreme precipitation events are affected by different SST patterns. Generally, a small difference [for median value, (max − min)/min < 10%] was found in RX1day and R99p indices, but a relatively large difference [for median value, (max − min)/min > 10%] was found in the PRCPTOT, SDII, CDD, and R10mm indices. The largest increase in future precipitation amount (PRCPTOT) is observed from the HA pattern, the median of which is up to approximately 850 mm. The lowest increase is projected from GF pattern, the median of which is up to approximately 780 mm.

c. *Assessment of benefits from a large ensemble*

Besides the high resolution, the power of a large ensemble in d4PDF is the improvement in estimations of the mean and of statistical distributions. For brevity,

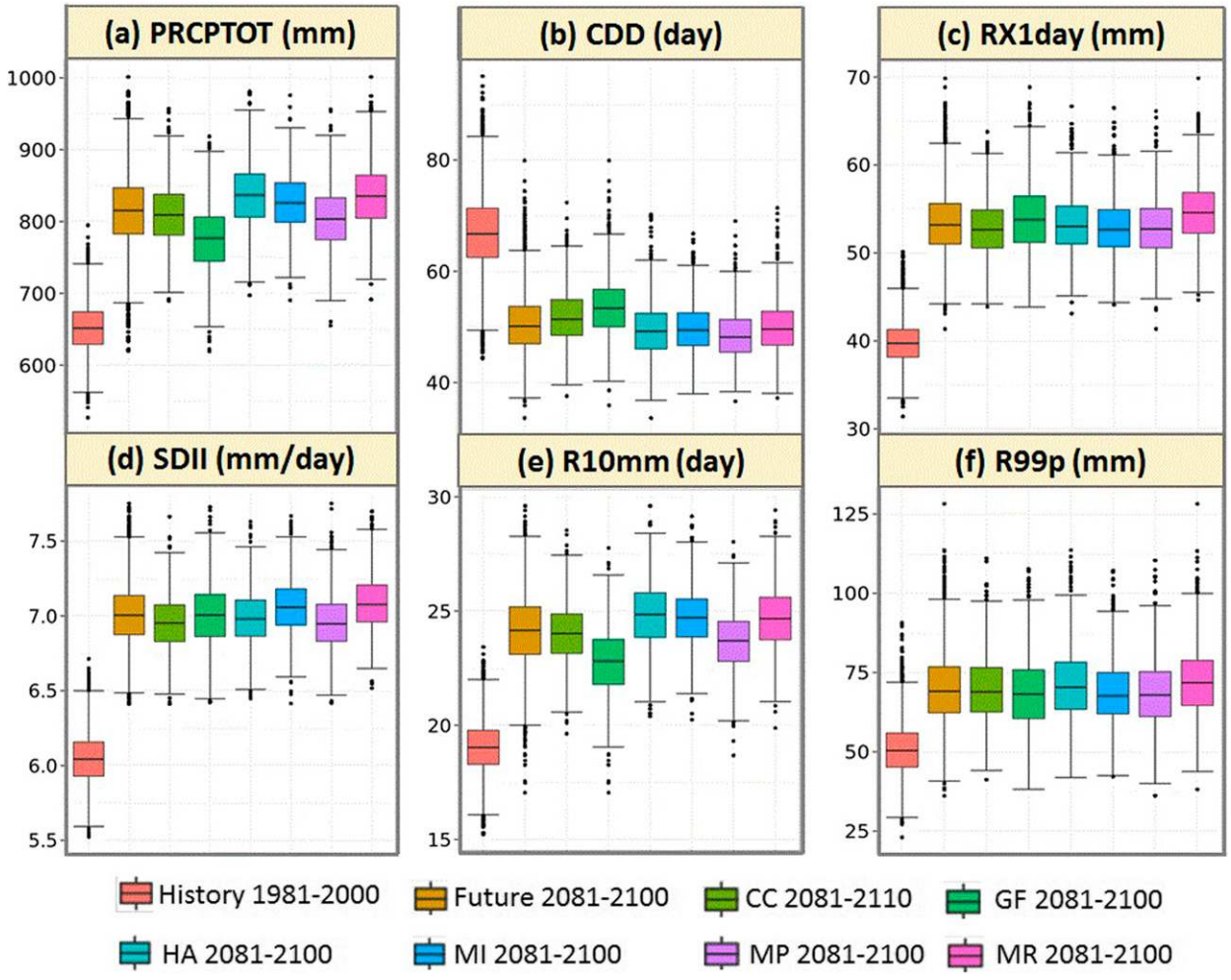

FIG. 8. Projected changes in all precipitation extremes over the period 2081–2100 relative to the reference period 1981–2000 along with each delta SST pattern separately. Boxes indicate the interquartile model spread (25th and 75th quartiles) with the horizontal line indicating the ensemble mean and the whiskers showing the extreme range of the d4PDF ensemble.

two indices, including PRCPTOT and SDII, were selected to show the range in simulated values of regional mean precipitation events with growing number of ensembles, averaged over all of China for one year (Fig. 9a). Figure 9a indicates that both the mean deviation and the tails of the distribution decrease rapidly with ensemble size, showing that one ensemble member would give us within −460 to +720 mm of the precipitation deviation for China, while it would be ±400 mm for 64 members. The same character can be found for SDII. These advantages illustrate that large ensemble simulations can reduce the uncertain range of impact-relevant extreme weather events and be used to conduct statistical analysis of extreme weather (Li et al. 2015) by improving the signal-to-noise ratio, especially for capturing the main features of subregions (O'Brien et al. 2011).

In addition, in Fig. 7, we can conclude that when all 100 historical ensemble members or 90 future ensemble members are applied to evaluate changes in indices measuring precipitation extremes, we can expect larger area with statistically significant changes compared to the area using one ensemble member. For example, areas with no statistical significance (shown in white) are widely distributed across China for R99p when using one ensemble member (Fig. 7f), while considerable areas show statistical significance (shown in colors) when using 100 or 90 ensemble members (Fig. 7f), similarly for both northwestern and southeastern China for CDD and SDII. This advantage may occur because the internal climate variability is simulated by the unique expression in only one ensemble member, but could be stated by lots of different expressions in a large ensemble, which is line with the results obtained from Kay et al. (2015) and Mote et al. (2016).

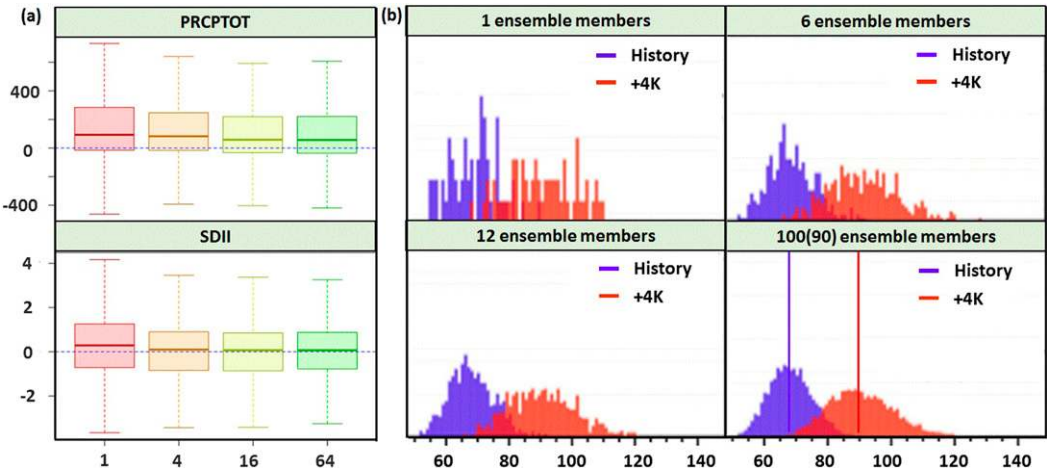

FIG. 9. (a) The distribution of the deviation, in the ensemble statistic from the population statistic with increasing ensemble size for (top) PRCPTOT and (bottom) SDII for 2010 for all of China. Samples of 1, 4, 16, and 64 members were randomly selected from a set of 100 simulations. (b) Frequency histogram of averaged maximum yearly precipitation between historical and +4-K future in southern China. The color lines represent the mean value.

With a large number of ensemble members, d4PDF also has the ability to better simulate and predict the probability of extreme climate events, which is shown in Fig. 9b. From the figure, we can see that the result from one ensemble member can capture only a small part of the character of averaged annual maximum daily precipitation between the historical period and a +4-K future in southern China, such that the accurate probability of extreme climate events could not be obtained. With the increase in the number of ensemble members, however, the map of frequency histograms becomes smoother, and it is clear when using 100 or 90 ensemble members. So, by using a large ensemble, d4PDF provides one possible way to accurately estimate the probability of extreme precipitation in both history and future, and the averaged annual maximum daily precipitation will be likely to increase by approximately 18% under +4-K future in southern China compared to the past.

d. Uncertainty analysis for future projection

Figure 10a shows spatial distribution of the total variance $\hat{\sigma}_{\text{tot}}$ among all 90 ensemble members (15 ensemble members × 6 SST patterns) for the PRCPTOT), the value of which is ~30% in northwestern China and ~8% in southeastern China. The variance $\hat{\sigma}_{\text{tot}}$ contains two parts: one is the component caused by the difference in six ΔSST patterns $\hat{\sigma}_{\Delta\text{SST}}$ (Fig. 10a) and the other is caused by the internal variability among 15 ensemble ensembles $\hat{\sigma}_{\text{int}}$ (Fig. 10a). Figure 10a shows the ratio of $\hat{\sigma}_{\Delta\text{SST}}$ to $\hat{\sigma}_{\text{int}}$, which suggests that variances caused by the difference in six ΔSST patterns are larger than those due to internal variability arising from the chaotic nature of the atmosphere over China, especially in southern China. The uncertainty in southern China is also more strongly influenced by differences in ΔSST patterns than the internal variability for the extreme precipitation indices (Fig. 10b). These results clearly indicate the uncertainty in model simulations for China, even with higher regional spatial resolution used in this research (Endo et al. 2017; Mizuta et al. 2017). Differences in ΔSST patterns are likely to affect precipitation through tropical cyclones and the Asian monsoon, which is the main reason why more rainfall is generally expected to hit southern, southeastern, and eastern China (Ren et al. 2006).

To better understand the regional differences, two regions with large uncertainty, southern China (20°–27°N, 106°–120°E) and the Qinghai–Tibet area (27°–36°N, 77°–106°E), were selected to compare regional averages of $\hat{\sigma}_{\text{tot}}$, $\hat{\sigma}_{\Delta\text{SST}}$, and $\hat{\sigma}_{\text{int}}$ for extreme precipitation indices (Fig. 10c). Except for Rx1day and CDD, the regional magnitude of average uncertainty value in the Qinghai–Tibet area is greater than for southern China, especially for R10mm and R99p, revealing a great deal of complexity and uncertainty in GCM future extreme precipitation events simulation at high altitudes. The SST pattern $\hat{\sigma}_{\Delta\text{SST}}$ is the major source of uncertainty for PRCPTOT in these two areas, revealing that SST patterns in tropical sea are likely to bring about the changes of larger-scale circulation (e.g., Asian monsoon activity) and may be the main factor for precipitation changes. For consecutive dry days (CDD), $\hat{\sigma}_{\Delta\text{SST}}$ is higher than $\hat{\sigma}_{\text{int}}$ in southern China, but the opposite is true in the Qinghai–Tibet area, indicating that the main source of uncertainty may be different in the eight regions

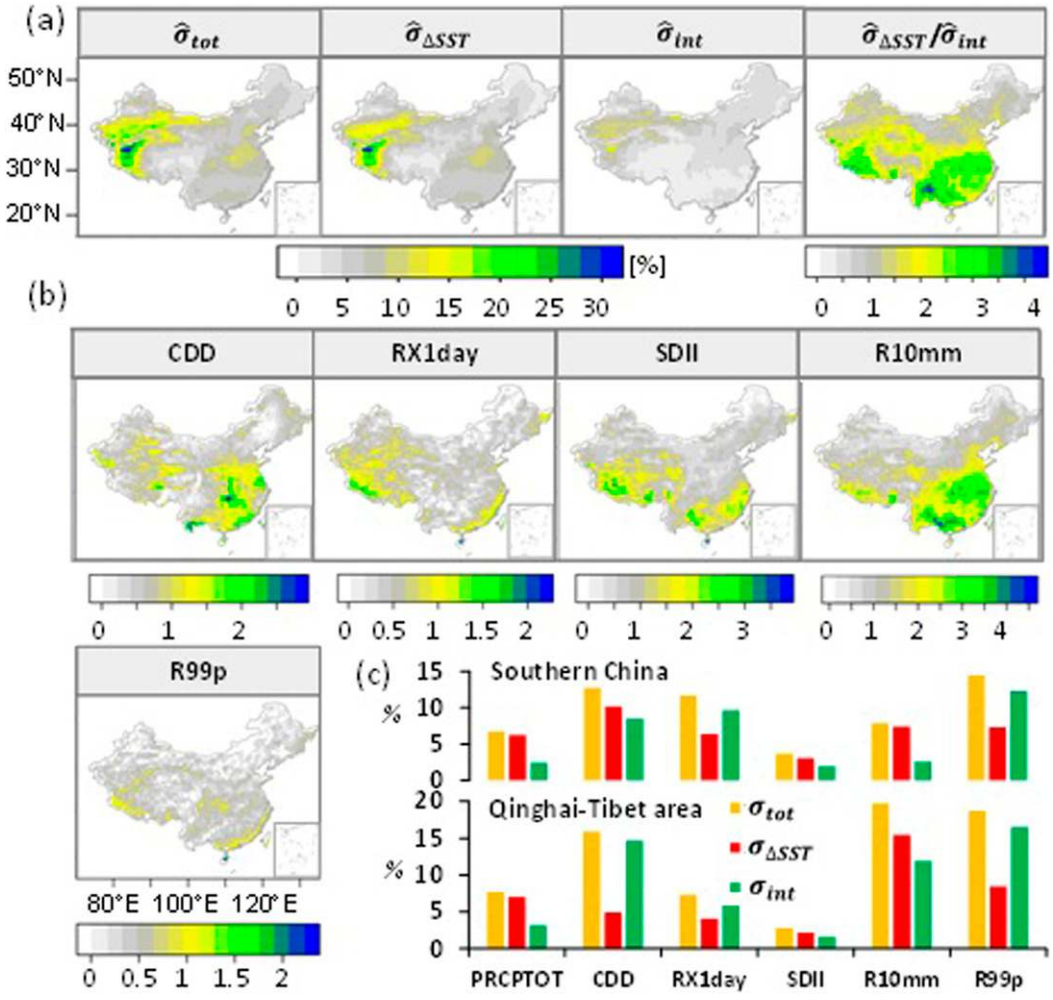

FIG. 10. (a) Decomposing of uncertainty for future PRCPTOT: (left to right) the component of ensemble spread among all members $\hat{\sigma}_{\text{tot}}$ (%), the component due to the difference in ΔSST patterns $\hat{\sigma}_{\Delta\text{SST}}$ (%), the component due to the internal variability seen in the 15 ensemble members $\hat{\sigma}_{\text{int}}$ (%), and the ratio of $\hat{\sigma}_{\Delta\text{SST}}$ to $\hat{\sigma}_{\text{int}}$, in using analysis of variance (ANOVA) without replication. (b) The ratio of $\sigma_{\Delta\text{SST}}$ to σ_{int} for precipitation extreme indices. (c) Area-averaged values of σ_{tot}, $\sigma_{\Delta\text{SST}}$, and σ_{int} for the extreme precipitation indices over southern China (20°–27°N, 106°–120°E) and the Qinghai–Tibet area (27°–36°N, 77°–106°E). Note that all the values are first calculated on the original grid and then averaged over the domains.

of China. These results could be useful when developing and improving the AGCMs with high-resolution atmospheric models to ensure realistic SST patterns (Endo et al. 2012; Wuebbles et al. 2014) and some climate phenomena (e.g., El Niño) (Thirumalai et al. 2017) for projections.

4. Conclusions

This study evaluated properties of the precipitation indices of China as simulated by a high-resolution AGCM with a large ensemble of projections. The major findings of this study are summarized as follows: 1) the overall trend and magnitude of precipitation amounts and extreme precipitation events were reasonably well characterized by the historic projections for China for all four seasons, which is better than the historical simulation of CMIP5, suggesting that the high-resolution AGCM can represent localized precipitation extremes without applying any statistical bias correction; 2) d4PDF future projections for 4-K-warmer climates had higher resolution and made distinguishing changes for eight subregions compared to the RCP8.5 of CMIP5 simulations; 3) the potential power of a large-ensemble was demonstrated in improving simulation precision in both the precipitation mean and the precipitation extremes; also, the averaged maximum yearly precipitation will be likely to increase by approximately 18% under +4-K future in southern China

compared to the past; and 4) uncertainty in future precipitation projections was evaluated, suggesting that the component caused by the difference in six ΔSST patterns is more important for total precipitation in southern China compared with that due to internal variability. The uncertainty should be further studied combined with tropical cyclones in future.

Acknowledgments. This study was supported by the Strategic Priority Research Program of the Chinese Academy of Sciences (Grant XDA19030204), the National Natural Science Foundation of China (Grant 41501552), the Natural Science Foundation of Jiangsu Province (Grant BK20161612), the Thousand Youth Talents plan of China, and the CAS Pioneer Hundred Talents Program. The d4PDF dataset can be accessed at http://search.diasjp.net/en/dataset/d4PDF_GCM.

REFERENCES

Bader, D. C., C. Covey, W. J. Gutowski Jr., I. M. Held, K. E. Kunkel, R. L. Miller, R. T. Tokmakian, and M. H. Zhang, 2008: Climate models: An assessment of strengths and limitations. U.S. Climate Change Science Program and the Subcommittee on Global Change Research, 123 pp., https://science.energy.gov/~/media/ber/pdf/Sap_3_1_final_all.pdf.

Chen, H., J. Sun, X. Chen, and W. Zhou, 2012: CGCM projections of heavy rainfall events in China. *Int. J. Climatol.*, **32**, 441–450, https://doi.org/10.1002/joc.2278.

Christidis, N., G. S. Jones, and P. A. Stott, 2015: Dramatically increasing chance of extremely hot summers since the 2003 European heatwave. *Nat. Climate Change*, **5**, 46–50, https://doi.org/10.1038/nclimate2468.

Collins, M., and Coauthors, 2013: Long-term climate change: Projections, commitments and irreversibility. *Climate Change 2013: The Physical Science Basis*, T. F. Stocker et al., Eds., Cambridge University Press, 1029–1136, https://www.ipcc.ch/pdf/assessment-report/ar5/wg1/WG1AR5_Chapter12_FINAL.pdf.

Duan, W., B. He, K. Takara, P. Luo, M. Hu, N. E. Alias, and D. Nover, 2015: Changes of precipitation amounts and extremes over Japan between 1901 and 2012 and their connection to climate indices. *Climate Dyn.*, **45**, 2273–2292, https://doi.org/10.1007/s00382-015-2778-8.

——, ——, D. Nover, J. Fan, G. Yang, W. Chen, H. Meng, and C. Liu, 2016: Floods and associated socioeconomic damages in China over the last century. *Nat. Hazards*, **82**, 401–413, https://doi.org/10.1007/s11069-016-2207-2.

Endo, H., A. Kitoh, T. Ose, R. Mizuta, and S. Kusunoki, 2012: Future changes and uncertainties in Asian precipitation simulated by multiphysics and multi–sea surface temperature ensemble experiments with high-resolution Meteorological Research Institute atmospheric general circulation models (MRI-AGCMs). *J. Geophys. Res.*, **117**, D16118, https://doi.org/10.1029/2012JD017874.

——, ——, R. Mizuta, and M. Ishii, 2017: Future changes in precipitation extremes in East Asia and their uncertainty based on large ensemble simulations with a high-resolution AGCM. *SOLA*, **13**, 7–12, https://doi.org/10.2151/sola.2017-002.

Fischer, E. M., and R. Knutti, 2015: Anthropogenic contribution to global occurrence of heavy-precipitation and high-temperature extremes. *Nat. Climate Change*, **5**, 560–564, https://doi.org/10.1038/nclimate2617.

Freychet, N., S. Sparrow, S. Tett, M. J. Mineter, G. C. Hegerl, and D. Wallom, 2018: Impacts of anthropogenic forcings and El Niño on Chinese extreme temperatures. *Adv. Atmos. Sci.*, **35**, 994–1002, https://doi.org/10.1007/s00376-018-7258-8.

Imada, Y., S. Maeda, M. Watanabe, H. Shiogama, R. Mizuta, M. Ishii, and M. Kimoto, 2017: Recent enhanced seasonal temperature contrast in Japan from large ensemble high-resolution climate simulations. *Atmosphere*, **8**, 57, https://doi.org/10.3390/atmos8030057.

Ji, Z., and S. Kang, 2015: Evaluation of extreme climate events using a regional climate model for China. *Int. J. Climatol.*, **35**, 888–902, https://doi.org/10.1002/joc.4024.

Jones, P. W., 1999: First- and second-order conservative remapping schemes for grids in spherical coordinates. *Mon. Wea. Rev.*, **127**, 2204–2210, https://doi.org/10.1175/1520-0493(1999)127<2204:FASOCR>2.0.CO;2.

Kay, J. E., and Coauthors, 2015: The Community Earth System Model (CESM) large ensemble project: A community resource for studying climate change in the presence of internal climate variability. *Bull. Amer. Meteor. Soc.*, **96**, 1333–1349, https://doi.org/10.1175/BAMS-D-13-00255.1.

Kiktev, D., J. Caesar, L. V. Alexander, H. Shiogama, and M. Collier, 2007: Comparison of observed and multimodeled trends in annual extremes of temperature and precipitation. *Geophys. Res. Lett.*, **34**, L10702, https://doi.org/10.1029/2007GL029539.

Li, S., P. W. Mote, D. E. Rupp, D. Vickers, R. Mera, and M. Allen, 2015: Evaluation of a regional climate modeling effort for the western United States using a superensemble from weather@home. *J. Climate*, **28**, 7470–7488, https://doi.org/10.1175/JCLI-D-14-00808.1.

Li, Z., X. Xu, M. Liu, X. Li, R. Zhang, K. Wang, and C. Xu, 2017: State-space prediction of spring discharge in a karst catchment in southwest China. *J. Hydrol.*, **549**, 264–276, https://doi.org/10.1016/j.jhydrol.2017.04.001.

Massey, N., and Coauthors, 2015: weather@home—Development and validation of a very large ensemble modelling system for probabilistic event attribution. *Quart. J. Roy. Meteor. Soc.*, **141**, 1528–1545, https://doi.org/10.1002/qj.2455.

Matsueda, M., and H. Endo, 2017: The robustness of future changes in Northern Hemisphere blocking: A large ensemble projection with multiple sea surface temperature patterns. *Geophys. Res. Lett.*, **44**, 5158–5166, https://doi.org/10.1002/2017GL073336.

Mizuta, R., and Coauthors, 2012: Climate simulations using MRI-AGCM3. 2 with 20-km grid. *J. Meteor. Soc. Japan*, **90**, 233–258, https://doi.org/10.2151/jmsj.2012-A12.

——, and Coauthors, 2017: Over 5000 years of ensemble future climate simulations by 60-km global and 20-km regional atmospheric models. *Bull. Amer. Meteor. Soc.*, **98**, 1383–1398, https://doi.org/10.1175/BAMS-D-16-0099.1.

Mote, P. W., M. R. Allen, R. G. Jones, S. Li, R. Mera, D. E. Rupp, A. Salahuddin, and D. Vickers, 2016: Superensemble regional climate modeling for the western United States. *Bull. Amer. Meteor. Soc.*, **97**, 203–215, https://doi.org/10.1175/BAMS-D-14-00090.1.

National Report Committee, 2007: *China's National Assessment Report on Climate Change* (in Chinese). Science Press, 422 pp.

New, M., M. Hulme, and P. Jones, 2000: Representing twentieth-century space–time climate variability. Part II: Development of 1901–96 monthly grids of terrestrial surface climate. *J. Climate*,

13, 2217–2238, https://doi.org/10.1175/1520-0442(2000)013<2217:RTCSTC>2.0.CO;2.

O'Brien, T. A., L. C. Sloan, and M. A. Snyder, 2011: Can ensembles of regional climate model simulations improve results from sensitivity studies? *Climate Dyn.*, **37**, 1111–1118, https://doi.org/10.1007/s00382-010-0900-5.

Ren, F., G. Wu, W. Dong, X. Wang, Y. Wang, W. Ai, and W. Li, 2006: Changes in tropical cyclone precipitation over China. *Geophys. Res. Lett.*, **33**, L20702, https://doi.org/10.1029/2006GL027951.

Schaller, N., and Coauthors, 2016: Human influence on climate in the 2014 southern England winter floods and their impacts. *Nat. Climate Change*, **6**, 627–634, https://doi.org/10.1038/nclimate2927.

Seneviratne, S. I., and Coauthors, 2012: Changes in climate extremes and their impacts on the natural physical environment. *Managing the Risks of Extreme Events and Disasters to Advance Climate Change Adaptation*, C. B. Field et al., Eds., Cambridge University Press, 109–230,.

Shiogama, H., and Coauthors, 2016: Attributing historical changes in probabilities of record-breaking daily temperature and precipitation extreme events. *SOLA*, **12**, 225–231, https://doi.org/10.2151/sola.2016-045.

Sillmann, J., V. V. Kharin, X. Zhang, F. W. Zwiers, and D. Bronaugh, 2013: Climate extremes indices in the CMIP5 multimodel ensemble: Part 1. Model evaluation in the present climate. *J. Geophys. Res.*, **118**, 1716–1733, https://doi.org/10.1002/jgrd.50203.

Su, F., X. Duan, D. Chen, Z. Hao, and L. Cuo, 2013: Evaluation of the global climate models in the CMIP5 over the Tibetan Plateau. *J. Climate*, **26**, 3187–3208, https://doi.org/10.1175/JCLI-D-12-00321.1.

Sugi, M., R. Kawamura, and N. Sato, 1997: A study of SST-forced variability and potential predictability of seasonal mean fields using the JMA global model. *J. Meteor. Soc. Japan*, **75**, 717–736, https://doi.org/10.2151/jmsj1965.75.3_717.

Sun, Y., X. Zhang, F. W. Zwiers, L. Song, H. Wan, T. Hu, H. Yin, and G. Ren, 2014: Rapid increase in the risk of extreme summer heat in eastern China. *Nat. Climate Change*, **4**, 1082–1085, https://doi.org/10.1038/nclimate2410.

Tang, J., X. Niu, S. Wang, H. Gao, X. Wang, and J. Wu, 2016: Statistical downscaling and dynamical downscaling of regional climate in China: Present climate evaluations and future climate projections. *J. Geophys. Res.*, **121**, 2110–2129, https://doi.org/10.1002/2015JD023977.

Taylor, K. E., 2001: Summarizing multiple aspects of model performance in a single diagram. *J. Geophys. Res.*, **106**, 7183–7192, https://doi.org/10.1029/2000JD900719.

Thirumalai, K., P. N. DiNezio, Y. Okumura, and C. Deser, 2017: Extreme temperatures in Southeast Asia caused by El Niño and worsened by global warming. *Nat. Commun.*, **8**, 15531, https://doi.org/10.1038/ncomms15531.

Wu, J. and X. Gao, 2013: A gridded daily observation dataset over China region and comparison with the other datasets (in Chinese). *Chinese J. Geophys.*, **56**, 1102–1111, https://doi.org/10.6038/cjg20130406.

Wu, Y., and Coauthors, 2019: The characteristics of regional heavy precipitation events over eastern monsoon China during 1960–2013. *Global. Planet. Change*, **172**, 414–427, https://doi.org/10.1016/j.gloplacha.2018.11.001.

Wuebbles, D., and Coauthors, 2014: CMIP5 climate model analyses: Climate extremes in the United States. *Bull. Amer. Meteor. Soc.*, **95**, 571–583, https://doi.org/10.1175/BAMS-D-12-00172.1.

Xu, Y., X. Gao, Y. Shen, C. Xu, Y. Shi, and F. Giorgi, 2009: A daily temperature dataset over China and its application in validating a RCM simulation. *Adv. Atmos. Sci.*, **26**, 763–772, https://doi.org/10.1007/s00376-009-9029-z.

Yin, Z., X. Zhang, X. Liu, M. Colella, and X. Chen, 2008: An assessment of the biases of satellite rainfall estimates over the Tibetan Plateau and correction methods based on topographic analysis. *J. Hydrometeor.*, **9**, 301–326, https://doi.org/10.1175/2007JHM903.1.

Yoshida, K., M. Sugi, R. Mizuta, H. Murakami, and M. Ishii, 2017: Future changes in tropical cyclone activity in high-resolution large-ensemble simulations. *Geophys. Res. Lett.*, **44**, 9910–9917, https://doi.org/10.1002/2017GL075058.

Zhai, P., and X. Pan, 2003: Trends in temperature extremes during 1951–1999 in China. *Geophys. Res. Lett.*, **30**, 1913, https://doi.org/10.1029/2003GL018004.

Zhang, X., L. Alexander, G. C. Hegerl, P. Jones, A. K. Tank, T. C. Peterson, B. Trewin, and F. W. Zwiers, 2011: Indices for monitoring changes in extremes based on daily temperature and precipitation data. *Wiley Interdiscip. Rev.: Climate Change*, **2**, 851–870, https://doi.org/10.1002/wcc.147.

Zhang, Y., Y. Xu, W. Dong, L. Cao, and M. Sparrow, 2006: A future climate scenario of regional changes in extreme climate events over China using the PRECIS climate model. *Geophys. Res. Lett.*, **33**, L24702, https://doi.org/10.1029/2006GL027229.

Zhou, B., Q. H. Wen, Y. Xu, L. Song, and X. Zhang, 2014: Projected changes in temperature and precipitation extremes in China by the CMIP5 multimodel ensembles. *J. Climate*, **27**, 6591–6611, https://doi.org/10.1175/JCLI-D-13-00761.1.

——, Y. Xu, J. Wu, S. Dong, and Y. Shi, 2016: Changes in temperature and precipitation extreme indices over China: Analysis of a high-resolution grid dataset. *Int. J. Climatol.*, **36**, 1051–1066, https://doi.org/10.1002/joc.4400.